Phys Chem Minerals (2006) 33: 289–299
DOI 10.1007/s00269-005-0045-y

ORIGINAL PAPER

Chul-Min Chon · Chul-Kyoo Lee · Yungoo Song
Sin Ae Kim

Structural changes and oxidation of ferroan phlogopite with increasing temperature: in situ neutron powder diffraction and Fourier transform infrared spectroscopy

Received: 11 December 2004 / Accepted: 15 October 2005 / Published online: 19 May 2006

Abstract The thermal response of the natural ferroan phlogopite-1*M*, $K_2(Mg_{4.46}Fe_{0.83}Al_{0.34}Ti_{0.22})(Si_{5.51}Al_{2.49})O_{20}[OH_{3.59}F_{0.41}]$ from Quebec, Canada, was studied with an in situ neutron powder diffraction. The in situ temperature conditions were set up at −263, 25, 100°C and thereafter at a 100°C intervals up to 900°C. The crystal structure was refined by the Rietveld method ($R_p = 2.35$–2.78%, $R_{wp} = 3.01$–3.52%). The orientation of the O–H vector of the sample was determined by the refinement of the diffraction pattern. With increasing temperature, the angle of the OH bond to the (001) plane decreased from 87.3 to 72.5°. At room temperature, a = 5.13 Å, b = 9.20 Å, c = 10.21 Å, β = 100.06° and V(volume) = 491.69 Å^3. The expansion rate of the unit cell dimensions varied discontinuously with a break at 500°C. The shape of the M-octahedron underwent some significant changes such as flattening at 500°C. At temperatures above 500°C, the octahedral thickness and mean <M–O> distance was decreased, while the octahedral flattening angle increased. Those results were attributed to the Fe oxidation and dehydroxylation processes. The dehydroxylation mechanism of the ferroan phlogopite was studied by the Fourier transform infrared spectroscopy (FTIR) after heated at temperatures ranging from 25 to 800°C with an electric furnace in a vacuum. In the OH stretching region, the intensity of the OH band associated with Fe^{2+} (N_B-band) begun to decrease outstandingly at 500°C. The changes of the IR spectra confirmed that dehydroxylation was closely related to the oxidation in the vacuum of the ferrous iron in the M-octahedron. The decrease in the angle of the OH bond to the (001) plane, with increasing temperature, might be related to the imbalance of charge in the M-octahedra due to Fe oxidation.

Keywords Ferroan phlogopite · Neutron powder diffraction · FTIR · Oxidation · Dehydroxylation

C.-M. Chon
Korea Institute of Geoscience and Mineral Resources, Daejeon 305-350, Korea

C.-K. Lee · Y. Song (✉)
Department of Earth System Sciences, Yonsei University, 134, Shinchondong Seodaemungu, 120-749 Seoul, Korea
E-mail: yungoo@yonsei.ac.kr
Tel.: +82-2-21232671
Fax: +82-2-3926527

S. A. Kim
Korea Atomic Energy Research Institute, Daejeon 305-353, Korea

Introduction

Recent studies for trioctahedral micas have been focused on Fe oxidation effect for the three-dimensional cation ordering and the orientation and dehydroxylation of OH group with increasing temperature (Pavese et al. 1997, 1999, 2000; Mookerjee et al. 2001; Chon et al., 2003). For this, in situ high-temperature neutron diffraction study with several supplementary equipments, such as Fourier transform infrared spectroscopy (FTIR), mössbauer spectroscopy, should be employed.

Since the first study on the structural changes of mica at high temperature by Takeda and Morosin (1975), various high-temperature structural studies have been conducted. Guggenheim et al. (1987) studied the dehydroxylation of the muscovite at high temperature, and Russell and Gugenheim (1999) along with Tutti et al. (2000) reported the crystal structures of phlogopite at high temperature. All these studies were performed by X-ray diffraction (XRD). Because X-rays are scattered by electrons, H and/or D atoms cannot always be observed even at high resolution with X-ray analyses. On the other hand, neutrons scattered by atomic nuclei can directly provide a large quantity of information about light atoms, and then the neutron diffraction has many advantages over XRD, such as its weak absorption, high penetration and angle-independent scattering length. Rayner (1974) and Joswig (1972) studied the crystal structure of the phlogopite at

room temperature using neutron single diffraction. Either room-temperature or low-temperature neutron powder diffraction was also used for the accurate determination of crystal structures, especially for investigating the positions of the H atoms in structure (Catti et al. 1994; Pavese et al. 2001; Rancourt et al. 1994).

In spite of the many previous works on micas (Takeda and Morosin 1975; Russell and Guggenheim 1999; Tutti et al. 2000), high-temperature structural study for Fe-bearing trioctahedral mica was rarely attempted, because of complications, such as Fe oxidation and dehydroxylation, associated with the oxidation process. Chon et al. (2003) examined Fe-rich phlogopite at in situ high temperatures and also performed a room temperature structural study of ex situ furnace heating samples using neutron powder diffraction. However, they just observed that the Fe oxidation and dehydroxylation in octahedra for the ex situ heat-treated Fe-rich phlogopite, but could not confirm the oxidation process at in situ high temperature. The dehydroxylation of Fe-bearing trioctahedral mica at high temperature also has been studied by several investigators using FTIR and mössbauer spectroscopy. Vedder and Wilkins (1969) showed that biotite can be oxidized without changes in its layer structure at high temperatures in an oxidizing atmosphere. Tripathi et al. (1978) suggested that a decrease in the octahedral dimension of Fe-bearing phlogopite in vacuum conditions at high temperature could be caused by a dehydroxylation–oxidation reaction of Fe^{2+} to Fe^{3+}. Hogg and Meads (1975) and Sanz et al. (1983) also investigated the structural Fe oxidation of heat-treated biotite in both air and vacuum environments. In these previous works, it was clearly evident that the structural Fe oxidation of the biotite began to occur at about 400°C in air condition with increasing temperature. However, Hogg and Meads (1975) reported that no oxidation occurred in a vaucum setting, while Sanz et al. (1983) suggested that Fe oxidation might occur at higher temperatures (600–800°C) even in a vacuum. In addition they did not reveal the Fe oxidation effects on structural changes including OH bond orientation and dehydroxylation processes.

Therefore, the aim of our work was to study the structural changes of the Fe-bearing phlogopite at in situ high temperatures and to determine the significance of the changes including OH bond orientation with relation to the Fe oxidation and dehydroxylation in vacuum condition. For the study, in situ neutron powder diffraction at high temperature and Rietveld refinement methods were employed for the accurate determination of the crystal structure for Fe-bearing phlogopite. In addition, FTIR was used to investigate the dehydroxylation mechanism related to Fe oxidation for the sample heated at different temperatures in vacuum condition.

Experimental method

A natural ferroan phlogopite-1 *M* sample, $K_2(Mg_{4.46}Fe^{2+}_{0.83}Al_{0.34}Ti_{0.22})(Si_{5.51}Al_{2.49})O_{20}[(OH_{3.59})F_{0.41}]$ from Quebec, Canada was collected for this study. The bulk chemical composition of the phlogopite was determined using an electron probe micro-analysis (SX-50, CAMECA) at the Korea Basic Science Institute. The structural formula was calculated on the basis of the electron-microprobe data, on the assumption that the iron is in a +2 oxidation (ferrous) state. The phlogopite sample was ground in a vibrating milling machine and dry-sieved. The 20–50 μm fraction was used for the neutron powder diffraction and FTIR study.

Neutron powder diffraction

A high resolution powder diffractometer (HRPD) at Hanaro, Korea Atomic Energy Research Institute, was used to obtain neutron diffraction data. The neutron wavelength was 1.836Å, which was selected by a Ge(331) monochrometor. The 4.3 g of phlogopite powder was loaded into a vanadium container, which had a 12 mm diameter and a length of 55 mm, within sample environments. The cryostat (closed cycle refrigerator) with Si diode sensor was used to control the sample temperature at −263°C. The high-temperature sample environments were controlled with a heating rate of 1°C/min in the furnace with a vacuum of 10^{-3} Torr. Diffraction patterns were collected from 0 to 160° 2θ, with a step size 0.05° 2θ and a step monitoring count of 130,000 *n* using a He-3 proportional counter (32 multi-channel detector). The neutron data were collected at in situ different temperatures of −263°C, room temperature, 100, 200, 300, 400, 500, 600, 700, 800 and 900°C for 9 h under vacuum conditions(10^{-3} Torr).

The diffraction patterns were analyzed by the Rietveld method (Rietveld 1969) using the FullProf program (Rodriguez-Carvajal 1998). The initial atomic parameters of all refinements were obtained from the coordinate set determined by Chon et al. (2003). The peak shape profile was a peudo-Voigt function and the background was modeled with a polynminal function. The prefered orientations were taken into account using the March function (Dollase 1986) and the full with at half maximum (FWHM) was refined with three parameters *u*, *v* and *w* depending on 2θ (Cagliotti et al. 1958). All the data below 21° 2θ were excluded from the diffraction profiles due to the large degree of asymmetry, and the thermal parameters for all atoms were considered as isotropic. The global parameters (zero shift for 2θ, six background coefficients), scale factor, unit cell parameters and FWHM parameters, were varied first in a space group $C2/m$ with the positions reported by Chon et al. (2003). Subsequently, atomic positions and prefered orientation parameters were allowed to vary, and then site occupancies and isotropic thermal parameters were refined in succeeding cycles. Finally, the site occupancies, which did significantly differ between the refinements and the chemical analysis, were constrained according to the chemical analyses, and a total of 45 parameters were refined.

Fourier transform infrared spectroscopy (FTIR)

The phlogopite powder samples were heated for a period of 1 h at different temperatures over RT −800°C. At 10^{-3} Torr, a graphite vacuum furnace was used. The infrared (IR) spectra were collected on a Perkin Elmer FTIR spectrometer. The powdered samples were prepared as KBr pellets (25 mg of sample mixed with 300 mg of KBr). Those pellets were dried at 110°C for 2 h under vacuum to eliminate the absorbed water. The spectra fitting was done with the program PeakFit, version 4.11 and the peak-fit function was Guassian–Lorentzian Sum. The detailed fitting procedure was described in Redhammer et al. (2000). But it is difficult-to-impossible to fit a baseline in an objective and still in a persuasive manner (Hawthorne et al. 2000), and the final band intensities are slightly dependent on the set of the starting parameters (Redhammer et al. 2000). For those reasons, we also did not attempt a quantitative analysis but a qualitative interpretation of the band intensity.

Results

The agreement factors and experimental details of the Rietveld refinements are shown in Table 1 and the diffraction pattern at room temperature is illustrated in Fig. 1. The 345–363 unique reflections were separated in the 21–146° 2θ range at final refinements. The crystal structure was refined to an R_p of 2.42–3.48%, R_{wp} of 3.13–4.39%.

The unit cell dimensions, atomic coordinates and displacement factors(B_{iso}) for all the experimental sets are shown in Tables2 and 3. At room temperature, a = 5.313 Å, b = 9.204 Å, c = 10.209 Å, β = 100.06° and V(volume) = 491.61 Å^3. The c dimension of this phlogopite was larger than that of F-rich phlogopite (10.167(9)Å: Tutti et al. 2000; 10.134(1)Å: Takeda and Morosin 1975). This must be a consequence of the hydrogen-interlayer cation repulsion (Russell and Guggenheim 1999). With increasing temperature, the dimensions a, b and c increased. Although the expansion rate of c increased linearly, those of a and b decreased after the 500°C mark as illustrated in Fig. 2. The β unit cell parameter increased below 500°C, but decreased above 500°C (Fig. 2). The thermal expansivities $\alpha_x = (1/X_{25})(X_T - X_{25})/(T-25)$°C (Takeda and Morosin 1975) along c, a and b were, respectively, 1.71×10^{-5}°C^{-1}, 1.14×10^{-5}°C^{-1} and 1.12×10^{-5}°C^{-1} between the 25 and 500°C range, and changed to 1.62×10^{-5}°C^{-1}, 0.71×10^{-5}°C^{-1} and 0.61×10^{-5}°C^{-1} between 500 and 800°C.

The final bond lengths and angles are given in Table 4. The interatomic distances were calculated with the FullProf program, the values of ρ, the angle that the OH vector makes with the (001) plane were calculated using cosine formula between OH vector and the c^* direction (M. Mookherjee, private communication). The structural parameters are given in Table 5.

In the IR spectra of the ferroan phlogopite, the OH-stretching region was more than 3,600–3,800 cm^{-1}. The spectra were dominated by one prominent band centered at around 3,712 cm^{-1}, and one additional band centered at around 3,668 cm^{-1}. These spectra bands of ferroan phlogopite were similiar to those of iron-free phlogopite reported by Wilkins (1967) and Vedder (1964). However, the samples investigated in this study showed considerable intensities at around 3,685 cm^{-1}. Those results must be attributed to the replacement of Mg^{2+} by Fe^{2+} in the octahedral site. Details of these bands and the spectra of the OH region when the applied temperature increased are shown in Fig. 3.

Table 1 Experimental details and final parameters of structure refinements

T(°C)	−263°C	25°C	100°C	200°C	300°C	400°C	500°C	600°C	700°C	800°C
Neutron data collection										
2°C scan range (°)					21–146					
Step size (°)					0.05					
No. of fitted parameters					45					
No. of reflections	345	346	346	352	354	354	355	356	360	363
$N - P + C$	2,393	2,454	2,454	2,454	2,454	2,454	2,454	2,454	2,454	2,454
Refinement index										
R_p (%)	2.42	3.30	3.28	3.31	3.36	3.40	3.39	3.43	3.35	3.48
R_{wp} (%)	3.13	4.22	4.19	4.26	4.28	4.33	4.34	4.32	4.23	4.39
R_{exp} (%)	1.44	1.68	1.69	1.69	1.70	1.70	1.70	1.71	1.72	1.73
S (G. of F.)	2.17	2.51	2.47	2.52	2.59	2.53	2.54	2.53	2.46	2.53
R_B (%)	4.05	7.05	7.05	7.13	7.51	8.04	8.77	9.81	9.88	10.8
R_F (%)	2.31	4.78	4.95	5.11	5.55	6.23	7.18	8.21	8.27	8.76
Full width at half maximum (FWHM)										
U	0.548 (9)	0.62 (1)	0.63 (1)	0.64 (1)	0.63 (1)	0.63 (1)	0.65 (2)	0.65 (2)	0.67 (2)	0.68 (2)
V	−0.59 (1)	−0.76 (2)	−0.78 (2)	−0.80 (2)	−0.80 (2)	−0.83 (2)	−0.87 (3)	−0.88 (3)	−0.90 (3)	−0.91 (3)
W	0.341 (6)	0.382 (9)	0.389 (9)	0.396 (9)	0.39 (1)	0.41 (1)	0.42 (1)	0.43 (1)	0.43 (1)	0.43 (1)

Note: $R_p = 100 \times |Y_{io} - Y_{ic}|/Y_{io}$ (R-pattern), $R_{wp} = 100 \times [w_i(Y_{io} - Y_{ic})^2/w_i Y_{io}^2]^{1/2}$ (R-weighted pattern), $R_B = 100 \times |\,|I_{Ko}| - |I_{Kc}|\,|/\,|I_{Ko}|$ (R-Bragg factor), $R_F = 100 \times |\,|I_{Ko}|^{1/2} - |I_{Kc}|^{1/2}|\,/\,|I_{Ko}|^{1/2}$ (R-structure factor), $H^2 = U\tan 2\theta + V\tan\theta + W$ (according to Young 1993)

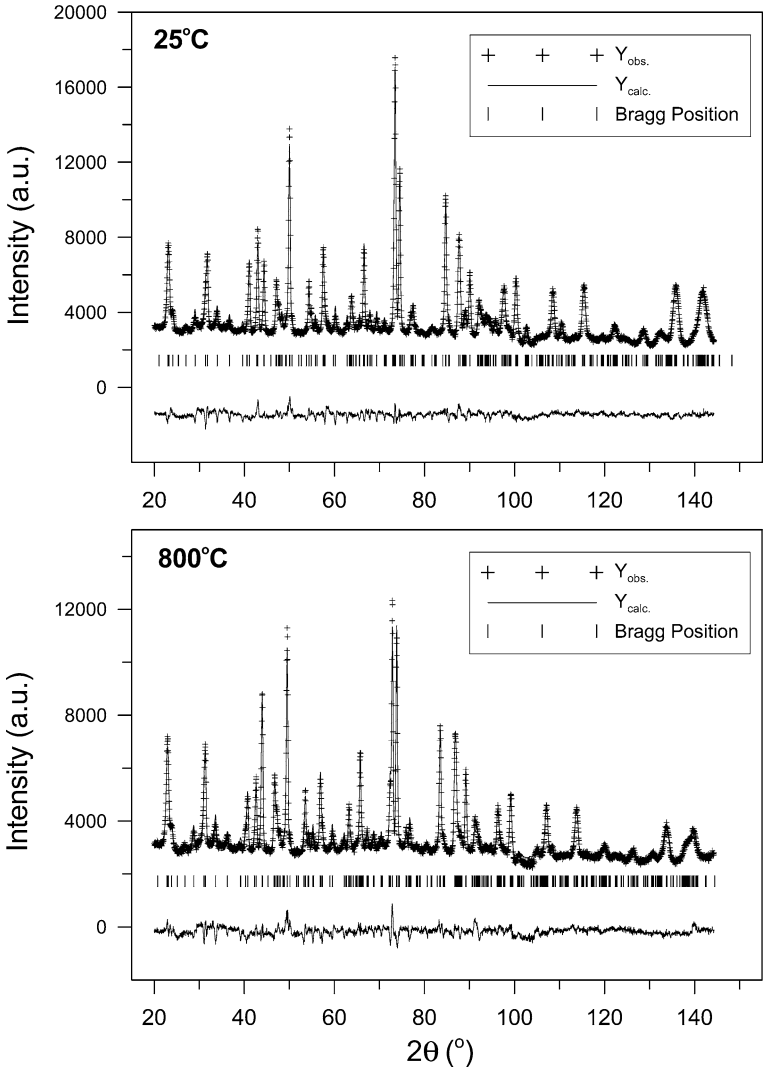

Fig. 1 Comparison of observed (*crosses*,Yobs) and calculated (*solid line*, Ycalc) neutron powder diffraction patterns of phlogopite at 25 and 800°C, determined by Rietveld refinement. The differences, observed minus calculated, are shown in the *lower field*. The *short vertical bars* indicate the positions of possible Bragg reflections

Discussion

Structural changes of phlogopite at high temperatures

Previous works (Takeda and Morosin 1975; Tutti et al. 2000) showed that the expansion rate of the F-rich phlogopite had a kink at about 400°C. They concluded that the mode controlling structural changes at temperatures above 400°C was quite different from that at temperatures below 400°C. An octahedron flattening angle, Ψ, is one of the structural parameters measuring structural changes. This angle is measured between the body diagonal and the normal to the top plane, and an

Table 2 Unit-cell parameters for phlogopite after final refinements

T(°C)	*a* (Å)	*b* (Å)	*c* (Å)	*β* (°)	*V* (Å^3)
−263	5.3022 (2)	9.1833 (4)	10.1795 (3)	100.078 (5)	488.01 (3)
25	5.3134 (3)	9.2042 (6)	10.2093 (4)	100.067 (7)	491.61 (5)
100	5.3181 (3)	9.2123 (6)	10.2202 (4)	100.070 (7)	492.99 (5)
200	5.3247 (4)	9.2245 (6)	10.2371 (4)	100.079 (7)	495.06 (5)
300	5.3312 (4)	9.2359 (6)	10.2541 (4)	100.084 (7)	497.10 (5)
400	5.3377 (4)	9.2455 (1)	10.2729 (5)	100.093 (6)	499.13 (6)
500	5.3427 (4)	9.2537 (7)	10.2923 (5)	100.092 (6)	500.98 (6)
600	5.3468 (4)	9.2616 (7)	10.3101 (5)	100.078 (7)	502.68 (6)
700	5.3497 (4)	9.2660 (7)	10.3250 (5)	100.075 (7)	503.93 (6)
800	5.3528 (5)	9.2708 (9)	10.3411 (6)	100.050 (8)	505.30 (7)
900	5.3558 (5)	9.2764 (9)	10.3594 (6)	100.010 (8)	507.22 (7)

Table 3 Positional cooridinates and displacement parameters for phlogopite after Rietveld refinement

		−263°C	25°C	100°C	200°C	300°C	400°C
T	*x*	0.072 (1)	0.075 (1)	0.076 (2)	0.074 (2)	0.075 (2)	0.078 (2)
	y	0.1674 (5)	0.1665 (7)	0.1664 (7)	0.1660 (8)	0.1653 (8)	0.1663 (9)
	z	0.2249 (3)	0.2246 (4)	0.2247 (4)	0.2254 (4)	0.2256 (4)	0.2259 (4)
	B_{iso}	0.91 (4)	0.88 (6)	0.95 (6)	0.98 (7)	1.07 (7)	1.08 (7)
M1	*x*	0	0	0	0	0	0
	y	0	0	0	0	0	0
	z	0.5	0.5	0.5	0.5	0.5	0.5
	B_{iso}	0.7 (1)	0.9 (1)	0.9 (1)	0.8 (1)	1.0 (1)	1.0 (1)
M2	*x*	0	0	0	0	0	0
	y	0.3301 (4)	0.3322 (5)	0.3320 (5)	0.3326 (6)	0.3330 (6)	0.3336 (7)
	z	0.5	0.5	0.5	0.5	0.5	0.5
	B_{iso}	0.66 (7)	0.44 (9)	0.5 (1)	0.5 (1)	0.7 (1)	0.9 (1)
K	*x*	0	0	0	0	0	0
	y	0.5	0.5	0.5	0.5	0.5	0.5
	z	0	0	0	0	0	0
	B_{iso}	0.1 (1)	2.0 (2)	2.5 (2)	3.1 (2)	4.0 (3)	4.4 (3)
O1	*x*	0.0015 (9)	0.004 (1)	0.008 (1)	0.015 (1)	0.022 (1)	0.026 (1)
	y	0	0	0	0	0	0
	z	0.1651 (5)	0.1630 (9)	0.1634 (9)	0.163 (1)	0.164 (1)	0.164 (1)
	B_{iso}	0.95 (6)	2.1 (2)	2.3 (2)	2.5 (2)	2.8 (2)	3.0 (2)
O2	*x*	0.3238 (8)	0.322 (1)	0.320 (1)	0.318 (1)	0.317 (1)	0.315 (1)
	y	0.2246 (2)	0.2294 (4)	0.2311 (4)	0.2332 (4)	0.2357 (4)	0.2388 (5)
	z	0.1677 (3)	0.1706 (5)	0.1712 (5)	0.1719 (5)	0.1725 (5)	0.1734 (6)
	B_{iso}	0.95 (6)	1.32 (9)	2.3 (2)	1.6 (1)	1.8 (1)	2.1 (1)
O3	*x*	0.1374 (9)	0.124 (2)	0.127 (2)	0.124 (2)	0.123 (1)	0.123 (1)
	y	0.1663 (3)	0.1672 (3)	0.1672 (4)	0.1668 (5)	0.1665 (5)	0.1671 (6)
	z	0.3911 (2)	0.3907 (3)	0.3905 (3)	0.3909 (3)	0.3904 (3)	0.3909 (3)
	B_{iso}	0.23 (4)	0.47 (6)	0.59 (6)	0.74 (6)	0.88 (7)	1.07 (7)
O4/F	*x*	0.143 (1)	0.131 (2)	0.133 (2)	0.130 (2)	0.130 (2)	0.132 (2)
	y	0.5	0.5	0.5	0.5	0.5	0.5
	z	0.4012 (5)	0.4000 (7)	0.3997 (7)	0.39886 (7)	0.3995 (7)	0.4001 (7)
	B_{iso}	0.82 (8)	1.4 (1)	1.5 (1)	1.5 (1)	1.6 (1)	2.1 (1)
H	*x*	0.099 (2)	0.093 (3)	0.092 (3)	0.095 (3)	0.092 (3)	0.091 (4)
	y	0.5	0.5	0.5	0.5	0.5	0.5
	z	0.298 (1)	0.305 (2)	0.306 (2)	0.308 (3)	0.311 (3)	0.303 (3)
	B_{iso}	1.8 (8)	4.2 (14)	6.2 (16)	6.7 (18)	8.8 (22)	13.5 (25)

		500°C	600°C	700°C	800°C
T	*x*	0.079 (2)	0.080 (2)	0.081 (2)	0.077 (2)
	y	0.1660 (9)	0.165 (1)	0.165 (1)	0.164 (1)
	z	0.2255 (5)	0.2249 (5)	0.2239 (5)	0.2238 (5)
	B_{iso}	1.1 (8)	1.30 (8)	1.47 (8)	1.54 (9)
M1	*x*	0	0	0	0
	y	0	0	0	0
	z	0.5	0.5	0.5	0.5
	B_{iso}	1.0 (2)	1.2 (2)	1.1 (2)	1.1 (2)
M2	*x*	0	0	0	0
	y	0.3334 (7)	0.3330 (8)	0.3336 (8)	0.3341 (8)
	z	0.5	0.5	0.5	0.5
	B_{iso}	1.2 (1)	1.4 (1)	1.7 (1)	2.0 (1)
K	*x*	0	0	0	0
	y	0.5	0.5	0.5	0.5
	z	0	0	0	0
	B_{iso}	5.2 (3)	6.2 (4)	6.5 (4)	6.7 (4)
O1	*x*	0.031 (1)	0.036 (1)	0.042 (1)	0.039 (1)
	y	0	0	0	0
	z	0.163 (1)	0.162 (1)	0.165 (1)	0.165 (1)
	B_{iso}	3.0 (3)	3.1 (3)	2.6 (3)	3.0 (3)
O2	*x*	0.315 (1)	0.314 (1)	0.315 (1)	0.314 (1)
	y	0.2408 (5)	0.2421 (6)	0.2426 (6)	0.2435 (6)
	z	0.1737 (6)	0.1746 (7)	0.1734 (7)	0.1735 (7)
	B_{iso}	2.5 (1)	2.8 (1)	3.3 (1)	3.5 (1)

Table 3 (Contd.)

		500°C	600°C	700°C	800°C
O3	x	0.125 (1)	0.125 (2)	0.126 (1)	0.126 (2)
	y	0.1675 (6)	0.1677 (6)	0.1682 (6)	0.1684 (7)
	z	0.3913 (3)	0.3910 (4)	0.3914 (4)	0.3920 (4)
	B_{iso}	1.19 (7)	1.4 (8)	1.55 (8)	1.65 (8)
O4/F	x	0.132 (2)	0.133 (2)	0.131 (2)	0.135 (2)
	y	0.5	0.5	0.5	0.5
	z	0.4005 (8)	0.4027 (7)	0.4024 (8)	0.4040 (9)
	B_{iso}	2.5 (1)	2.8 (1)	3.0 (1)	3.4 (1)
H	x	0.084 (4)	0.068 (4)	0.063 (4)	0.047 (7)
	y	0.5	0.5	0.5	0.5
	z	0.305 (3)	0.307 (2)	0.312 (2)	0.309 (3)
	B_{iso}	15.9 (28)	31.4 (44)	39.7 (54)	57.7 (65)

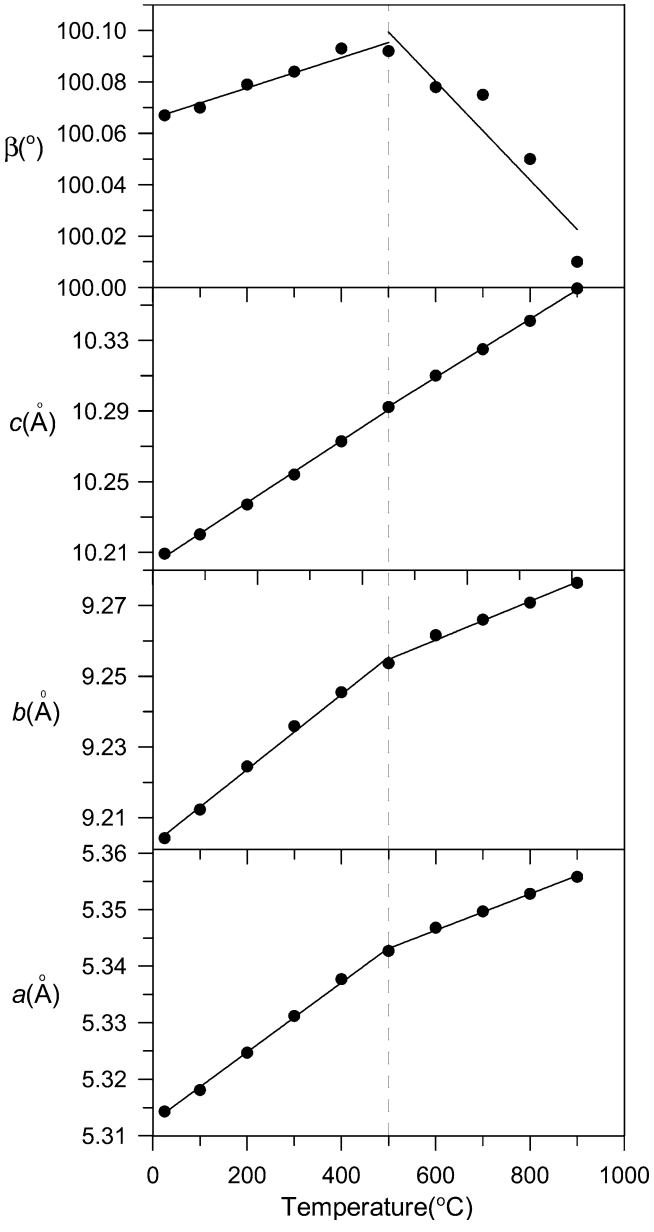

Fig. 2 Variation of a, b, c and °C with temperature for ferroan phlogopite. The *dashed line* indicates a break in slope at 500°C

ideal value would be 54.73. If the angle is greater than the ideal value, the octahedron is flattened, and the octahedral thickness is also reduced (Hazen and Burnham 1973). On the other hand, if the angle is smaller than the ideal value, the octahedron is elongated. Takeda and Morosin (1975) showed that the M-octahedron flattening angle did not have significant changes below 400°C, but above 400°C the M-octahedron flattening angle decreased rapidly. This suggested that at temperatures below 400°C the M-octahedron expanded without changing its shape. However, when the temperature increased above 400°C, the M-octahedra began to elongate more rapidly. Russell and Guggenheim (1999) also reported that the Mg octahedra (M1, M2) in an end-member phlogopite were flattened and essectially fixed in shape with temperature increasing between 20 and 600°C. Therefore, they could not observe any significant deviation of expansivities for cell parameter with increasing temperature.

In this study, data with a break in slope were obtained for the expansivities of the dimensions a and b. However, the kink of the expansivities was not observed at about 400°C but near 500°C. It was also interesting to find that the changes of the M-octahedron flattening angles were different from that of previous high-temperature structural studies (Takeda and Morosin 1975; Russell and Guggenheim 1999; Tutti et al. 2000). The $<$M–O$>$ distance increased more than the temperature range of 25–400°C, but nearly constant or rather slightly decreased for temperatures above that value (Fig. 4). The observed M-octahedron thickness slightly decreased at early stage and recovered initial room temperature value at 500°C, while they steeply decreased above 500°C. The M-octahedral flattening angle slightly increased to 300°C and recovered the initial value at 500°C. From that temperature, the distance value continuously decreased with increasing temperature. The results implied that M-octahedron began to seriously flatten at around 500°C. The variation of structural parameters over the temperature range of 25–400°C, results in a structural deformation to correct misfit, caused by thermal expansion, between octahedral and tetrahedral sheets.

Table 4 Calculated interatomic distances (Å) for phlogopite as determined from Rietveld refinement of neutron powder diffraction data

	−263°C	25°C	100°C	200°C	300°C	400°C	500°C	600°C	700°C	800°C
T–O1	1.633 (7)	1.612 (11)	1.607 (11)	1.617 (11)	1.622 (11)	1.608 (11)	1.609 (12)	1.602 (13)	1.604 (13)	1.624 (14)
T–O2	1.669 (7)	1.667 (10)	1.668 (10)	1.662 (10)	1.661 (11)	1.662 (11)	1.659 (12)	1.665 (13)	1.663 (12)	1.651 (14)
T–O2'	1.672 (5)	1.674 (7)	1.671 (8)	1.666 (8)	1.657 (8)	1.667 (9)	1.664 (9)	1.660 (10)	1.648 (10)	1.639 (10)
T–O3	1.666 (4)	1.670 (5)	1.668 (5)	1.669 (5)	1.664 (5)	1.669 (6)	1.680 (6)	1.687 (6)	1.704 (7)	1.713 (7)
<T–O>	1.660 (5)	1.656 (8)	1.654 (8)	1.654 (8)	1.651 (8)	1.651 (9)	1.653 (9)	1.653 (10)	1.655 (10)	1.657 (11)
M1–O3[x4]	2.091 (3)	2.075 (6)	2.077 (4)	2.076 (6)	2.079 (6)	2.082 (6)	2.089 (6)	2.095 (7)	2.100 (6)	2.100 (7)
M1–O4[x2]	1.981 (6)	2.044 (11)	2.055 (8)	2.056 (11)	2.058 (10)	2.048 (11)	2.050 (11)	2.037 (12)	2.050 (12)	2.028 (14)
<M1–O>	2.054 (4)	2.065 (7)	2.069 (5)	2.070 (7)	2.072 (7)	2.071 (7)	2.076 (7)	2.076 (8)	2.083 (8)	2.076 (9)
M2–O3[x2]	2.074 (4)	2.060 (7)	2.061 (5)	2.069 (7)	2.078 (7)	2.078 (8)	2.078 (8)	2.078 (9)	2.081 (8)	2.080 (9)
M2–O3'[x2]	2.043 (4)	2.109 (10)	2.107 (8)	2.112 (9)	2.120 (9)	2.121 (9)	2.114 (9)	2.116 (9)	2.112 (9)	2.111 (10)
M2–O4[x2]	2.070 (4)	2.040 (7)	2.057 (5)	2.048 (7)	2.042 (7)	2.042 (8)	2.043 (8)	2.039 (9)	2.033 (9)	2.031 (10)
<M2–O>	2.063 (4)	2.070 (8)	2.075 (6)	2.076 (7)	2.080 (7)	2.080 (8)	2.078 (8)	2.077 (9)	2.075 (9)	2.074 (10)
<M–O>	2.058 (4)	2.067 (7)	2.071 (5)	2.073 (7)	2.076 (7)	2.076 (7)	2.077 (7)	2.076 (8)	2.079 (8)	2.075 (9)
K–O1[x2]	2.886 (5)	2.897 (8)	2.919 (8)	2.956 (8)	2.992 (9)	3.013 (10)	3.038 (10)	3.056 (10)	3.098 (10)	3.091 (11)
K–O2[x4]	2.933 (3)	2.994 (4)	3.015 (4)	3.041 (5)	3.068 (5)	3.103 (5)	3.124 (6)	3.143 (6)	3.140 (6)	3.151 (7)
$<K–O>_{inner}$	2.917 (3)	2.962 (5)	2.983 (5)	3.013 (6)	3.042 (6)	3.073 (6)	3.095 (7)	3.114 (7)	3.126 (7)	3.131 (8)
K–O1[x2]	3.371 (5)	3.352 (7)	3.338 (8)	3.309 (8)	3.286 (9)	3.277 (9)	3.253 (10)	3.227 (10)	3.218 (10)	3.239 (11)
K–O2[x4]	3.351 (3)	3.335 (4)	3.324 (4)	3.314 (5)	3.302 (5)	3.285 (5)	3.275 (6)	3.272 (6)	3.267 (6)	3.262 (7)
$<K–O>_{outer}$	3.362 (3)	3.340 (5)	3.329 (5)	3.313 (6)	3.297 (6)	3.282 (6)	3.267 (7)	3.257 (7)	3.251 (7)	3.254 (8)
<O–H>	1.02 (1)	0.95 (2)	0.93 (2)	0.91 (3)	0.89 (3)	0.97 (3)	0.96 (3)	0.97 (2)	0.93 (2)	1.00 (3)
ρ	87.3 (3)	88.0 (2)	87.1 (2)	88.3 (2)	87.1 (2)	86.9 (2)	85.1 (2)	79.3 (2)	77.6 (2)	72.5 (2)

Table 5 Structural parameters for ferroan phlogopite

	−263°C	25°C	100°C	200°C	300°C	400°C	500°C	600°C	700°C	800°C
α^a (°)	5.79	4.62	4.31	3.84	3.27	2.55	2.09	1.79	1.67	1.47
Ψ (°)										
$\Psi^b_{Interlayer}$, Interlayer	55.00	55.21	55.34	55.55	55.74	55.88	56.09	56.21	56.29	56.22
Ψ^c_M, M-Octahedron	59.13	58.94	58.88	58.85	58.83	58.94	59.01	59.11	59.12	59.34
Interlayer separation (Å)	3.346	3.380	3.393	3.408	3.425	3.447	3.453	3.463	3.469	3.482
t^d_{oct}, Octaheron thickness (Å)	2.114	2.134	2.141	2.146	2.151	2.144	2.139	2.133	2.133	2.116

Notes: [a] α = tetrahedral rotation angle; $\tan\alpha = \frac{2b(0.25-y_{O2})}{0.5a}$

[b] $\Psi_{Interlayer}$ = K-octahedral flattening angle: $\cos\Psi = \frac{(K-octahedralthickness)}{2(mean_{inner}distance)}$ (according to Takeda and Donnay 1966)

[c] Ψ_M = octahedral flattening angle: $\cos\Psi = t_{oct}/2d_0$, d_0 = mean <M–O> distance (according to Hazen and Burnham 1973)

[d] t_{oct} = octahedron thickness; $t_{oct} = 2\left(0.5 - \frac{2(Z_{O3})+Z_{OH}}{3}\right)C_0 \sin\beta$

As noted earlier, the differences in the structural parameters from 500 to 900°C must be related to the dehydroxylation that was derived from the structural iron oxidation. The *a* and *b* dimensions decreased slightly at higher temperatures rather than increased, as observed at lower temperatures. This may be attributed to a change in the octahedral dimension caused by a dehydroxlation–oxidation reaction of Fe^{2+} to Fe^{3+} in vacuum conditions at the higher temperatures (Tripathi et al. 1978). The reaction is as follows:

$$[Fe^{2+} + OH^-]_{mica} \rightarrow [Fe^{3+} + O^{2-}]_{mica} + 1/2H_2 \quad (1)$$

The reduction of the M-octahedral thickness and <M–O> distance appeared to be caused by a change in the cation size (Fe^{2+} changed to Fe^{3+}) due to iron oxidation in octahedra (Chon et al. 2003). The reduction in M-octahedra of the phlogopite at temperatures above 500°C, confirmed our previous findings, which attributed the reduction process to the iron oxidation and dehydroxylation. These structural changes in the octahedra also played a role in the appearance of a kink in the expansion rate of the unit cell parameters near 500°C. The reduction trend of the mean <M–O> distance beginning at 500°C was in good agreement with the decrease trend in the expansion rates of parameters *a* and *b* at this temperature. However, Russell and Guggenheim (1999) could not observe the kink observed in this study, probably owing to the relatively high Fe content of our phlogopite. To verify the dehydroxylation in the structure, we attempted to refine by varying the occupancy of H site. The occupancies decreased with increasing in situ heating temperature, but the attempt to refine the occupancy was unstable since the values were meaningless or they diverged. Consequently, the present study could not provide detailed information on H occupancies.

Chon et al. (2003), Sanz et al. (1983) and Vedder and Wilkins (1969) found that the Fe oxidation of biotite begins at about 400°C in air. The dehydroxylation mechanisms of a biotite (Fe-rich phlogopite) at high temperature in air and in vacuum, were studied with the

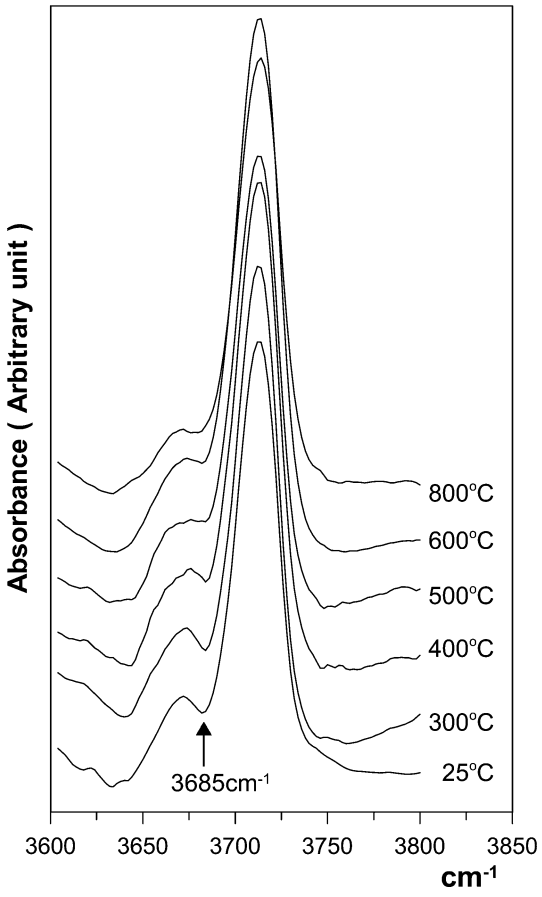

Fig. 3 The plot of Fourier transform infrared spectra (FTIR) corresponding to OH stretching region for ferroan phlogopite heated in vacuum with varying temperature

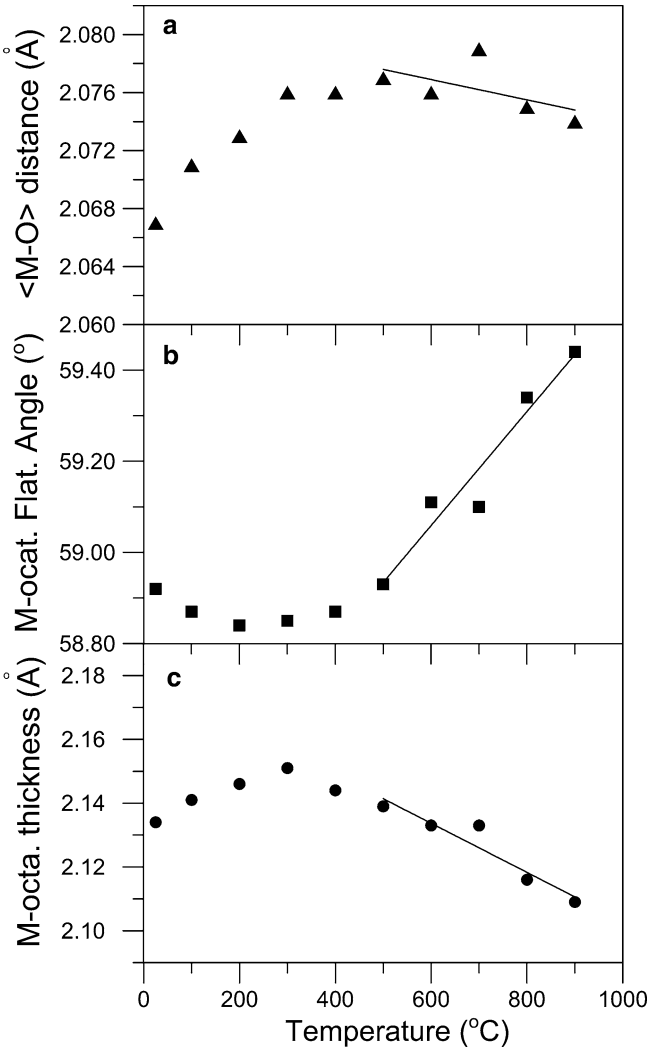

Fig. 4 Plots of **a** mean <M–O> distance, **b** M-octahedral flattening angle (Ψ), and **c** M-octahedral thickness as a function of temperature for ferroan phlogopite

combined use of IR and mössbauer spectroscpies (Sanz et al. 1983). They found a strong correlation between OH loss and Fe^{2+} oxidation in powder samples in both air and vacuum, and also verified that the dehydroxylation of biotite takes place at temperature higher than 400°C in vacuum. Vedder (1964) established the main features of the IR spectra of biotite. Three major bands were distinguished in the hydroxyl stretching region and were termed N, I and V bands (Wilkins 1967). The assignments are listed in Table 6. The IR spectra of our sample were fitted by these three N–I bands. The bands centered at around 3,712 and 3,696 cm^{-1} were assigned to N_A and N_B, respectively, and the other centered at around 3,668 cm^{-1} was assigned to I_A. At temperatures below 500°C, each band of OH-stretching regions showed no significant changes. For temperatures above 500°C, the intensity of the N_B band associated with Fe^{2+} decreased, but there was no significant changes in those of the other bands (Fig. 5). The decrease of the band indicated that the dehydoxylation related to Fe oxidation took place at this temperature. Therefore, those FTIR spectroscopic results also confirmed that the oxidation and dehydroxylation of the ferroan phlogopite took place at higher temperatures (500–800°C) and the dehydroxylation of the phlogopite was associated with Fe oxidation.

Hydroxyl behavior of phlogopite

Table 4 and Fig. 6 show the length and orientation of hydroxyl ion during heating. Because the proton was very light and vibarational, to obtain an acute information on hydroxyl ion, the experiment was performed at a very low temperature (−263°C) to minimize atom vibration. In concern with the results of the low temperature experiment, the length of OH was 1.02(1)Å and

Table 6 Assignments in the hydroxyl stretching region of phlogopite and biotite

Vibration frequency (cm^{-1})	Notation	Occupation of closest three octahedral sites		
3,712	N_A	Mg	Mg	Mg
3,696	N_B	Mg	Mg	Fe^{2+}
3,668	I_A	R^{3+}[a]	Mg	Mg

[a] R^3; Al, Fe^{3+} (according to Vedder 1964)

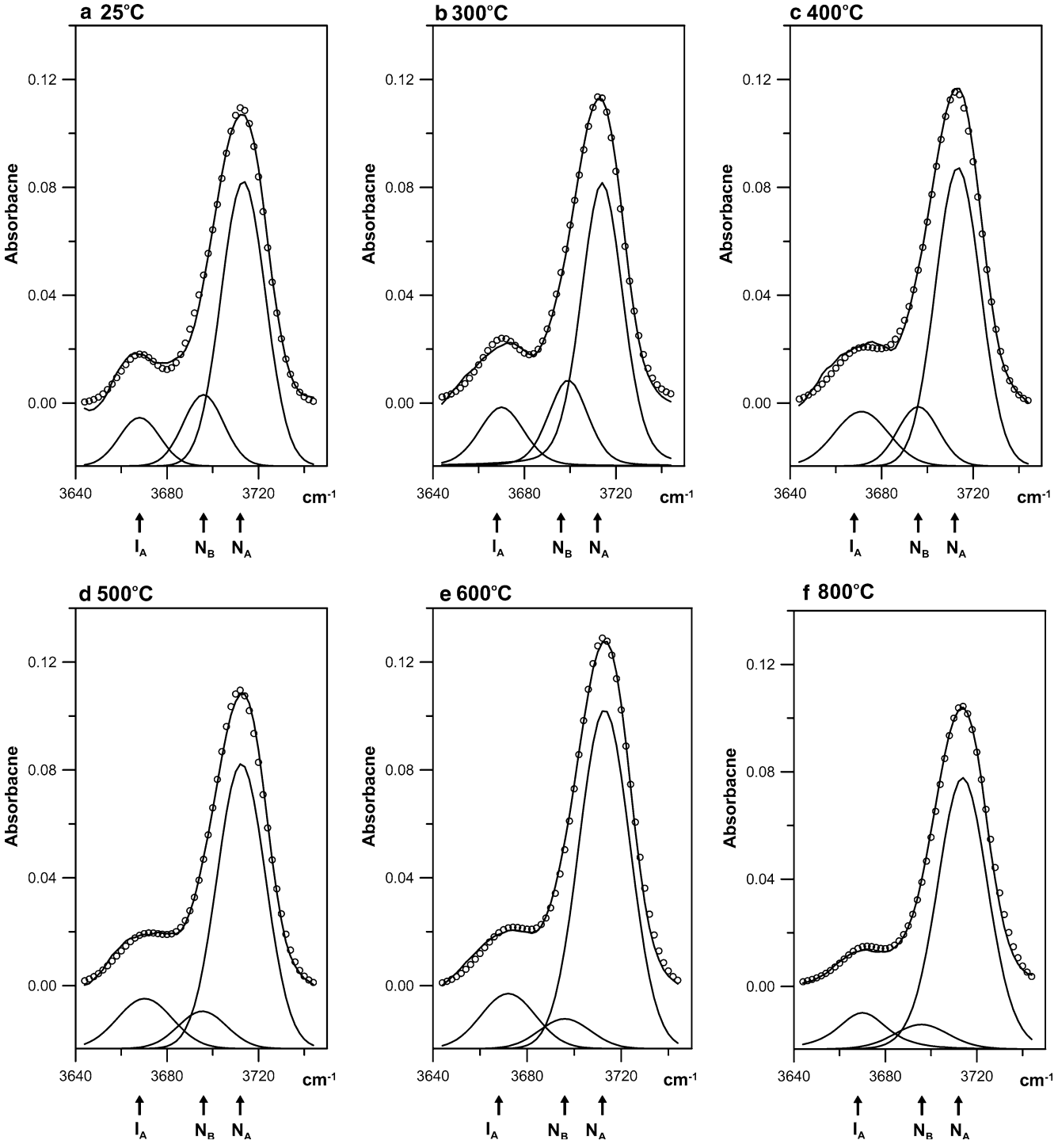

Fig. 5 The observed FTIR spectra of OH stretching region for ferroan phlogopite heated in vacuum at **a** room temperature **b** 300°C **c** 400°C, **d** 500°C, **e** 600°C, **f** 700°C, **g** 800°C and the calculated spectra fitted with the program PeakFit, version 4.11. The *lower lines* are the component bands; observed intensities are shown by *circles*, and the *line* following the observed intensities is the envelope of the sum of the fitted component bands

the orientation of OH, the angle (ρ) that the OH vector makes with the (001) plane was 87.3°.

In the trioctahedral mica structure, three cations of ocatahedron are symmetrically arranged around the OH. The OH directs away from the three M sites toward the interlayer cation, and the value of ρ is nearly 90° (Giese 1984). Previous studies of phlogopite by neutron diffraction (Rayner 1974; Joswig 1972) showed that the OH length is about 1.0 Å, and ρ is nearly perpendicular to the (001) plane. The angle, ρ was nearly 90° at tem-

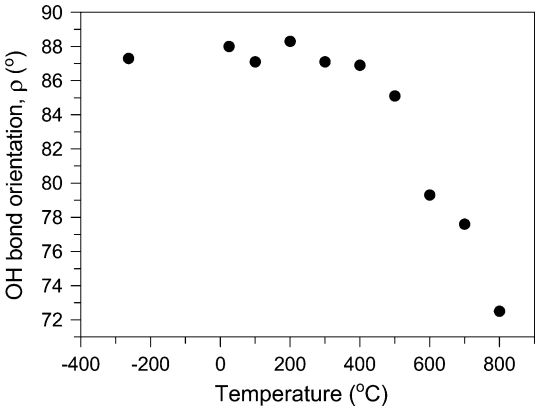

Fig. 6 Plot of the angles that O(4)-H vector makes with the (001) plane, as a function of temperature for ferroan phlogopite

peratures below 500°C, but above that value ρ decreased rapidly with increasing temperatures. At 800°C the angle was 72.5°. Mookerjee et al. (2001) showed that both the length and orientation of OH in phengite decreased. In the current study, however, there was no correlation between the OH bond length and increasing temperature. At temperatures above 600°C, the reduction of the angle ρ was also related to the reduction of M-octahedron, as mentioned earlier. It seems that the oxidation of Fe^{2+} to Fe^{3+} was the result of an imbalance of charge in octahedral sheet. The changes in the structure reoriented the hydroxyl ion.

Conclusion

This study found a kink in the expansion rate of unit cell dimensions at about 500°C by in situ neutron powder diffraction at high temperature. The structural parameters (M-octahedron flattening angle, M-octahedron thickness, <M–O> distance) also had significant changes at this temperature. The changes in the expansion mode must have been caused by the Fe oxidation and the dehydroxylation taking place in the mica structure. The IR specta bands of the OH-stretching regions confirmed that the dehydroxylation was closely related to the structural Fe oxidation of the mica powders that occurred at around 500°C in vacuum, because the intensities of the OH band (N_B) associated with Fe^{2+} began to decrease outstandingly at that temperature. With increasing temperature, the angle that the OH bond made with the (001) plane, decreased from nearly 90 to 72.5°. That result was estimated to be the result of an imbalance of layer charge in M-octahedra due to Fe oxidation.

Acknowledgements This research was supported by the Basic Research Project of the Korea Atomic Energy Research Institute (KAERI) and the Korea Institute of Geoscience and Mineral Resources (KIGAM) funded by the Ministry of Science and Technology of Korea.

References

Cagliotti G, Paoletti A, Ricci F (1958) Choice of collimators for a crystal spectrometer for neutron diffraction. Nucl Instrum 3:223–228

Catti M, Ferraris G, Hull S, Pavese, A (1994) Powder neutron diffraction study of $2M_1$ muscovite at room pressure and at 2 GPa. Eur J Miner 6:171–178

Chon C-M, Kim SA, Moon H-S (2003) Crystal structure of biotite at high temperatures and heat-treated biotite using neutron powder diffraction. Clays Clay Miner 51:519–528

Dollase WA (1986) Correction of intensities for preferred orientation in powder diffractometry: application of the march model. J Appl Cryst 19:267–272

Giese RF (1984) Electrostatic energy models of micas. Mineralogical Society of America. Rev Miner 13:105–144

Guggenheim S, Chang Y-H, Koster Van Groos AF (1987) Muscovite dehydroxylation: high-temperature studies. Am Miner 72:537–550

Hawthorne FC, Welch MD, Ventura GD, Liu S, Robert J-L, Jenkins DM (2000) Short-range order in synthetic aluminuous tremolites: an infrared and triple-quantum MAS NMR study. Am Miner 85:1716–1724

Hazen RM, Burnham CW (1973) The crystal structure of one-layer phlogopite and annite. Am Miner 58:889–900

Hogg CS, Meads RE (1975) A Mössbauer study of thermal decomposition of biotites. Min Mag 40:79–88

Joswig W (1972) Neutronenbeugungsmessungen an einem 1 *M*-Phlogopit. Neues Jahrb Min Monatsh 1–11

Mookerjee M, Redfern SAT, Zhang M (2001) Thermal response of structure and hydroxyl ion of phengite-$2M_1$: an in situ neutron diffraction and FTIR study. Eur J Miner 13:545–555

Pavese A, Ferraris G, Prencipe M, Ibberson R (1997) Cation site ordering in phengite 3 *T* from the dora-maira massif (western alps): a variable-temperature neutron powder diffraction study. Eur J Miner 9:1183–1190

Pavese A, Ferraris G, Pischedda V, Ibberson R (1999) Tetrahedral order in thermodynamic consequences. Eur J Miner 11:309–320

Pavese A, Ferraris G, Pischedda V, Radaelli P (2000) Further study of the cation ordering in phengite 3T by neutron powder diffraction. Min Mag 64:11–18

Pavese A, Ferraris G, Pischedda V, Fauth F (2001) M1-site occupancy in 3T and 2M(1) phengites by low temperature neutron powder diffraction: reality or artifact? Eur J Miner 13:1071–1078

Rancourt DG, Christie IAD, Lamarche G, Swainson I, Flandrois S (1994) Magnetism of synthetic and natural annite mica: ground state and nature of excitations in an exchange-wise two-dimensional easy-plane ferromagnet with disorder. J Magn Magn Mater 138:31–44

Rayner JH (1974) The crystal structure of phlogopite by neutron diffraction. Min Mag 39:850–856

Redhammer GJ, Beran A, Schneider J, Amthauer G, Lottermoser W (2000) Spectroscopic and structural properties of synthetic micas on the annite-siderophyllite binary: synthesis, crystal structure refinement, Mössbauer, and infrared spectroscopy. Am Miner 85:449–465

Rietveld HM (1969) A profile refinement method for nuclear and magnetic structures. J Appl Cryst 2:65–71

Rodriguez-Carvajal J (1998) FullProf: Rietveld profile matching and integrated intensity refinement of X-ray and neutron data (PC-version). Version 3.5d

Russell RL, Guggenheim S (1999) Crystal structures of near-end-member phlogopite at high temperatures and heat-treated Fe-rich phlogopite: the influence of the O, OH, F site. Can Miner 37:711–729

Sanz J, González-Carreño, Gancedo R (1983) On dehydroxylation mechanisms of a biotite in vacuo and in oxygen. Phys Chem Miner 9:14–18

Takeda H, Donnay JDH (1966) Trioctahedral one-layer micas. III. Crystal structure of a synthetic lithium fluormica. Acta Cryst 20:638–646

Takeda H, Morosin B (1975) Comparison of observed and predicted structural parameters of mica at high temperature. Acta Cryst B31:2444–2452

Tripathi RP, Chandra U, Chandra R, Lokanathan S (1978) A Mössbauer study of the effects of heating biotite, phlogopite and vermiculite. J Inorg Nucl Chem 40:1293–1298

Tutti F, Dubrovinsky LS, Nygren M (2000) High-temperature study and thermal expansion of phlogopite. Phys Chem Miner 27:599–603

Vedder W (1964) Correlations between infrared spectrum and chemical compostion of mica. Am Miner 49:736–768

Vedder W, Wilkins RWT (1969) Dehydroxylation and rehydroxylation, oxidation and reduction of micas. Am Miner 54:482–509

Wilkins RWT (1967) The hydroxyl-stretching region of the biotite mica spectrum. Min Mag 36:325–333

Young RA (1993) The rietveld method. International Union of Crystallography, Oxford University Press, Oxford, p 29